Effect of Different Promoter Precursors in a Model Ru-Cs/HSAG System on the Catalytic Selectivity for Fischer-Tropsch Reaction

José L. Eslava,[a] *Ana Iglesias-Juez,*[a] *Marcos Fernández-García,*[a,b] *Antonio Guerrero-Ruiz*[b,c] *and Inmaculada Rodríguez-Ramos*[*a,b]

[a] Instituto de Catálisis y Petroleoquímica, CSIC, C/Marie Curie 2, 28049 Madrid (Spain).

[b] Grupo de Diseño y Aplicación de Catalizadores Heterogéneos, Unidad Asociada UNED-CSIC (ICP), Spain.

[c] Departamento de Química Inorgánica y Química Técnica, UNED, C/ Senda del Rey 9, 28040 Madrid (Spain).

Corresponding author: I. Rodríguez-Ramos (e-mail: irodriguez@icp.csic.es)

ABSTRACT. The effect of the promoter precursor on the Fischer-Tropsch synthesis was studied over cesium promoted ruthenium catalysts supported on a high surface area graphite support. In this work we observe significant modifications in the selectivity values for Fischer-Tropsch reaction depending on the Cs promoter precursor (CsCl vs $CsNO_3$). Specifically the bimetallic catalyst (4Ru-4Cs), prepared from nitrogen containing metal and promoter precursors, showed a high selectivity to CO_2 during reaction. By modifying the cesium precursor, it was possible to inhibit the water gas shift reaction, decreasing significantly the selectivity to CO_2. In order to understand the chemical origin of these modifications a careful characterization of the materials was performed including: X-ray absorption near edge spectroscopy, transmission electron microscopy measurements, temperature programmed reduction studies, determination of the CO uptakes on the catalysts and the evolution of the CO adsorption heats as a function of surface coverages. It was found that upon reduction and under reaction atmosphere the promoter in the ex-nitrate catalyst appears as Cs_2O which is considered responsible of the CO_2 production, while in the catalysts prepared with Cs chloride the promoter remains as CsCl suffering a slight partial reduction.

KEYWORDS: Ruthenium and cesium precursors, electronic promoter, carbon materials, Fischer-Tropsch reaction.

1. INTRODUCTION

Fischer–Tropsch synthesis (FT) is an attractive reaction path to produce liquid fuels and chemicals from syngas (mixture of H_2 and CO) avoiding the use of petroleum resources, and leading the utilization of alternative row materials such as natural gas, coal or biomass. The FT product distribution is believed to follow the Anderson–Schulz–Flory (ASF) distribution [1, 2]. The most active metals in FT reaction are Ru, Co, Fe and Ni [1, 3, 4]. Under practical operating conditions Ni produces mainly CH_4 and tends to form nickel carbonyl species which are lost along the reaction. Fe and Co are commonly employed in the FT industry because of its activity, availability and price. Nevertheless, Ru catalysts despite its higher price possess some unique features in FT synthesis. It is the most active, working at the lowest reaction temperature and it produces the highest molecular weight hydrocarbons. It is appropriate for fundamental research to attain knowledge into the catalysts behavior and reaction mechanisms [5, 6, 7]. Furthermore Ru catalysts can be employed under higher partial pressures of water or other oxygenate-containing environment showing a good stability to deactivation under FT conditions.

Alkali promoters are usually utilized in FT with the aim of increasing both the activity and selectivity to high molecular weight hydrocarbons, and because these promoters favor the formation of olefins [8, 9]. It has been suggested that alkali elements (Na, K or Cs) increase the CO dissociative adsorption rate, resulting in an increase in the surface coverage of dissociated CO. Other groups have suggested that the alkali is an electronic promoter which donates part of its electron density to Ru, even in its oxidized state, producing the strengthening of the CO-metal interaction whereas the C-O bond is weakened [9,10,11,12]. Recently, some experimental evidences of the partial Cs reduction, under Fischer Tropsch synthesis conditions, have been revealed using X-ray absorption spectroscopy [13].

In general the support materials can play a crucial role on the reducibility of the metals, modifying activity and selectivity properties of the active phase and altering promoter effects

[14,15]. Carbons materials are promising supports for FT catalysts because the interaction between active metals and carbon surfaces is limited, compared to the strong interaction and even the formation of mixed compounds between metals and typical metal oxide supports, such as Al_2O_3, SiO_2, and TiO_2. In addition, carbon supports exhibit good hydrothermal stability [16] and the surface and textural properties of carbons can be easily adapted according to the requirements for obtaining a desired product. Also the inertness of the carbon surfaces facilitates the reduction of the metal precursor to the zero valence state and favors the interaction metal-promoter instead of the metal-support one [5,17]. In the present study, among the different available carbon materials, a high surface area graphite was selected, due to its high external surface area without presence of micropores. These latter pores could become saturated with the liquid products of the FT synthesis reaction, decreasing the transport of reactants and products from catalytic sites, and therefore altering the rate of primary and secondary reactions [18].

On the other hand, the selection of the metal and promoter precursors is also an important issue for designing FT catalysts. It might affect the intrinsic reactivity of the active centers located on the catalyst surface during Fischer-Tropsch synthesis [19,20,21]. So the type of metal precursor used in the preparation of the catalyst has a significant effect on the metal-support interactions, altering reduction properties of the metal and modifying final dispersion of metallic clusters. Besides, residual species from precursor (such as Cl^-) could remain anchored on the metal after the reduction step [7] blocking or modifying some adsorption active sites over the catalyst. Also the preparation method [22,23,24] has a remarkable influence on the way that catalytic species interact with the support and their reducibility. In addition, the pretreatment conditions [25,26] exert an important effect on the final catalyst properties due to changes or loss of active sites produced along the process. Consequently, all these factors can influence on the FT catalysts performance giving place to changes in terms of activity and selectivity.

In the present work different ruthenium and cesium precursors were used in the preparation of Ru-Cs catalysts supported on a high surface area graphite and the effect on their performance in the Fischer-Tropsch synthesis has been studied. It was observed that when cesium promoter is added (both for chloride or nitrate precursors) the selectivity of the reaction was modified toward higher molecular weight hydrocarbons and the formation of olefins was increased. The bimetallic catalyst (4%Ru-exnitroxyl nitrate-4%Cs-ex nitrate) showed a high value of CO_2 in FT reaction. By changing the cesium precursor for cesium chloride it was attained an inhibition of the water gas shift (WGS) reaction. In order to understand the reasons of these modifications a careful characterization of the materials was performed including in situ studies such as, X-ray absorption near edge spectroscopy (Ru K and Cs L_1 edges), transmission electron microscopy and CO chemisorption coupled with microcalorimetry.

2. EXPERIMENTAL SECTION

2.1 Catalyst Preparation

The selected catalyst support was a high surface area graphite provided by Timcal (S_{BET} = 399 $m^2 \cdot g^{-1}$). The incorporation of ruthenium was carried out using two different precursors: $Ru(NO)(NO_3)_3$ from Alfa-Aesar and $RuCl_3$ xH_2O from Aldrich. Cesium was employed as promoter and two precursors were also used: $Cs(NO_3)$ and CsCl, both obtained from Aldrich. All the catalysts were prepared by the incipient wetness impregnation method using a solution of ethanol-water (1:1) with the adequate concentration of the salts to incorporate 4 wt% Ru and/or 4 wt% of Cs to the support. After impregnation, the catalysts were kept at room temperature overnight and later heated at 393 K during 24h. The following abbreviations are used for precursors in conjunction with the catalyst: N for nitrates and Cl for chlorides compounds. The loading of ruthenium and cesium in the catalysts was determined by total reflection X-ray fluorescence (TRXF). Table 1 summarizes the chemical composition of the prepared catalysts.

Table 1. Ruthenium and cesium loading for all catalysts determined by TRXF.

Catalyst	Ru (wt%)	Cs (wt%)
4Ru-N	3.7	-
4Ru-Cl	3.6	-
4Ru-N-4Cs-N	4.2	3.8
4Ru-Cl-4Cs-Cl	3.6	3.4
4Ru-N-4Cs-Cl	3.6	3.6
4Cs-Cl	-	3.7
4Cs-NO	-	3.6

2.2 Catalyst Characterization

Temperature-programmed reduction (TPR) measurements were carried out in a U-shaped quartz microreactor with 200–300 mg of prepared sample, under a continuous flow of 60 ml/min of a H_2/Ar gas mixture (5% H_2). The temperature was increased from room temperature to 750 K at 5 K/min. H_2 consumption, as well as decomposition products (CO, CO_2 and CH_4), were measured by using an on-line gas chromatograph (Varian 3400) provided with a thermal-conductivity detector (TCD), an automatic sample injection and a Porapak Q column.

The CO uptake and the evolution of the CO chemisorption heats were recorded in a Tian Calvet heat-flow microcalorimeter (Setaram C-80 II) isothermally operated at 331 K and connected to a glass vacuum-dosing apparatus. Before starting the measure, the catalyst was reduced at 673 K during 2 h and then outgassed during 12 h at the same temperature. The metal surface was studied by treating the samples with successive pulses of the CO probe gas. Metal dispersion was calculated from the CO uptake assuming a molar stoichiometry CO/Ru = 1/1. It was considered to be achieved the monolayer when the evolved heat falls to the physisorption field (40 kJ mol^{-1}).

Transmission electron microscopy (TEM) measurements of the used catalysts were undertaken using a JEOL JEM-2100 field emission gun electron microscope operated at 200 kV. The samples were ground and ultrasonically suspended in hexane before deposition over a copper

grid with carbon coated layers. Ru particle diameter (d_{TEM}) was calculated based on a minimum of 350 particles (Table 2) using the following equation [27]:

$$d_{TEM} = \frac{\sum_i n_i d_i^3}{\sum_i n_i d_i^2} \quad (1)$$

Where n_i is the number of particles with diameter d_i. The dispersion values were calculated from the mean metal crystallite sizes assuming the spherical model, d_{TEM} (nm) = 1.32/D [28]

X-ray absorption measurements at Ru K edge (22.117 eV) were recorded in dispersive mode at EDXAS_L branch from beamline ID24 of the European Synchrotron Radiation Facility (ESRF, Grenoble, France). The catalysts were sieved to a size between 0.160 and 0.180 mm and then were placed in a fixed bed of a plug-flow microreactor system. The temperature was raised at 5 K min^{-1} up to 673 K using a flow of 11 cm^3 min^{-1} (10% H_2/He). XANES spectra were acquired every 10 K or 2 min during the heating process. Cs L_1 edge XANES spectra were recorded in transmission mode at beamline BL22-CLAESS of the ALBA Synchrotron (Barcelona, Spain). Samples were sieved to a 13 mm and loaded into a cell which was fed with 100 cm^3 min^{-1} of 20% H_2/He. The temperature was raised at 5 K min^{-1} up to 673 K. Every 15 K or 3 min XANES spectra were collected.

2.3 Catalytic Measurements

FT experiments were carried out in a stainless steel fix-bed reactor (length: 47 cm; inner diameter: 0.95 cm), operating at 523 K and at two different pressures: 3.5 and 15 bar. The reactor was filled with 0.5 g of fresh catalyst, SiC and quartz wool plugs. Samples were first in situ activated by 10 cm^3_{STP} min^{-1} of H_2 for 2 h at 673 K increasing the temperature at 5 K/min followed by cooling down to 523 K under H_2 flow. Then it was raised the pressure, CO and He were gradually introduced to the feed stream at 523 K in order to reach its final concentration CO/H_2/He (5/10/30 ml/min). The ratio of H_2/CO was 2/1 and the total flow rate of 45 cm^3/min.

Selectivity data were collected when a pseudo-steady-state catalytic behavior was achieved after 9 or 50 h on-stream. The outlet gas was analyzed online with a Bruker GC-450 gas

chromatograph equipped with two thermal conductivity detectors for the analysis of permanent gases (H_2, CO, CH_4 and CO_2) and one flame ionization detector for C_1–C_9 hydrocarbons analysis. The CO conversion levels were maintained below 18% to ensure differential operation in the reactor therefore limiting the extent of secondary reactions.

3. RESULTS AND DISCUSION

3.1 Catalysts Characterization

Figure 1 shows the TPR profiles of the non-promoted and Cs promoted ruthenium catalysts. Ru-N and Ru-Cl monometallic catalysts show one peak of hydrogen consumption centered at 458 and 450 K respectively that can be assigned to the reduction of Ru^{3+} to Ru^o species [29]. When cesium promoter is added the temperature of ruthenium reduction shifted toward higher values in the range 480 to 501 K. This behaviour is due to the existing interaction between ruthenium and cesium salts which is favored on the carbon support owing to the non-interaction of these species with the graphite support. From the TPR experiments, it can be assured that all the catalysts are completely reduced during the treatment in hydrogen at 673 K previous to the FT reaction tests.

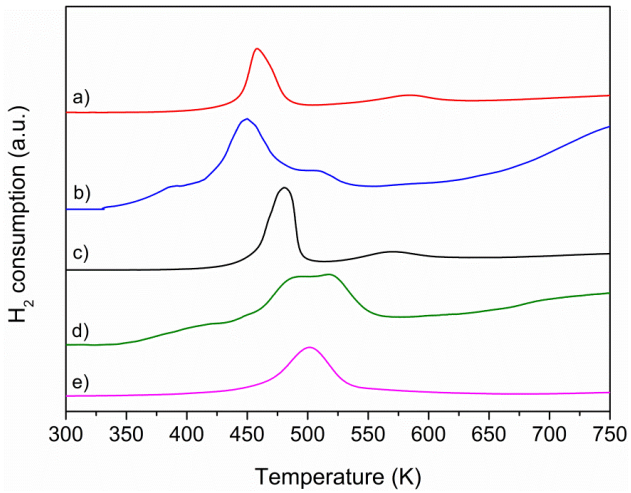

Figure 1. Hydrogen consumption profiles during temperature programmed reduction for the catalysts: a) 4Ru-N, b) 4Ru-Cl, c) 4Ru-N-4Cs-N, d) 4Ru-Cl-4Cs-Cl, e) 4Ru-N-4Cs-Cl.

Figure 2 presents the microcalorimetric CO adsorption profiles, which allow to obtain information about the strength and energetic distribution of the surface adsorption sites on the catalysts. It can be seen that adsorption heat profiles are different depending on the metal precursor as well as with the incorporation of promoter. 4Ru-N and 4Ru-Cl catalysts exhibit a high initial adsorption heat of 138 kJ/mol. This high value is associated with small ruthenium metal nanoparticles located preferentially at edges or corners where the coordination number is low. This initial adsorption heat quickly decreases to reach a constant value of 122 and 106 kJ/mol for 4Ru-N and 4Ru-Cl, respectively, for surface coverage from 0.2 to 0.7 and finally drops down to 40 kJ/mol (physisorption values). Thus, it has been detected that CO adsorption heats for 4Ru-N sample are higher than for 4Ru-Cl throughout the experiment. This finding agrees with previous results obtained over ex-choride Ru catalysts [30] and it can be explained because after pretreatment reduction step residual chlorine can remain on the catalyst surface removing electron density from the ruthenium metal nanoparticles and therefore CO adsorption heat on this catalyst is lower.

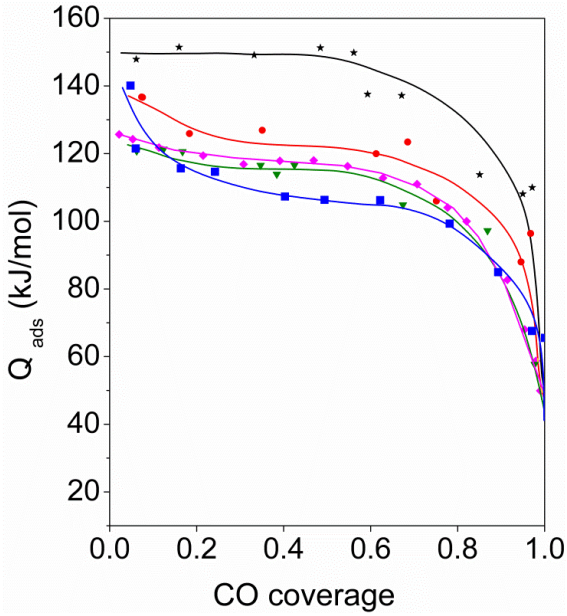

Figure 2. Differential CO adsorption heats at 331 K as a function of surface coverage for: (●) 4Ru-N, (■) 4Ru-Cl, (*) 4Ru-N-4Cs-N, (▼) 4Ru-Cl-4Cs-Cl and (◆) 4Ru-N-4Cs-Cl catalysts.

When cesium is added a diminution in the initial high heats of CO chemisorption is observed between 0.05-0.2 coverages. This fact suggests that Cs ions are likely localized on the highly reactive Ru positions blocking their adsorption properties. Moreover if the monometallic catalyst is compared with the promoted one, when using the same precursor (4Ru-Cl vs 4Ru-Cl-4Cs-Cl or 4Ru-N vs 4Ru-N-4Cs-N) it is revealed that the CO adsorption heats on promoted ruthenium catalyst are higher than those on non-promoted Ru catalysts. Cesium is believed to be an electronic promoter [10,11,31], because it donates part of its electron density to Ru nanoparticles, even in its oxidized form. A strengthening in the Ru-CO bond and higher CO adsorption heats is guessed due to such electronic transfer. On the other hand the sample 4Ru-N-4Cs-Cl shows a CO chemisorption profile very similar to 4Ru-Cl-4Cs-Cl with CO adsorption heats higher than that on 4Ru-Cl but below the 4Ru-N in the whole coverage range. This can be explained considering the residual chlorine withdraws electron density from the ruthenium nanoparticles decreasing the CO adsorption heats, as was explained above, partially neutralizing the promoter effect in the case of the 4Ru-N catalyst.

Representative TEM images of the catalysts and their histograms with particle size distributions are shown in Figure 3. Table 2 shows the CO uptakes and the average metal particle sizes (nm) obtained from chemisorption measurements and from TEM measurements for the non-promoted and Cs-promoted ruthenium catalysts. It is worth noting that CO uptakes grow for all promoted ruthenium catalysts with respect to the non-promoted catalysts which could have an important effect modifying the Fischer-Tropsch synthesis mechanism. It is observed for all the catalysts that particle sizes determined by CO chemisorption are larger than those obtained by TEM. A reason to explain this fact may rest on the considered adsorption stoichiometry of CO over Ru, since more than one Ru surface atom per chemisorbed CO molecule might be involved. So, we have considered a Ru-CO stoichiometry of 1:1 in order to calculate the number of Ru surface atoms and the metal dispersion, though CO adsorption in bridging configuration on two Ru atoms is also

possible and this would be reflected in larger average particle sizes of ruthenium. Therefore, due to these facts for comparison of the different catalysts we will use hereafter the metal dispersion derived from the metal particle sizes measured by TEM. In addition, TEM measurements reveal a broadening of the particle size distribution for all catalysts after the Cs addition (see figures 3a, 3b versus 3c, 3d and 3e), especially the frequency of particles larger than 2.5 nanometers.

Table 2. CO uptakes and average metal particle sizes obtained from CO chemisorption measurements and from TEM measurements after H_2 pretreatment at 673 K for 2 h.

Catalyst	CO uptake ($\mu mol/g_{cat}$)	d_{CO} (nm)	d_{TEM} (nm)
4Ru-N	115	4.1	1.7
4Ru-Cl	98	4.5	1.7
4Ru-N-4Cs-N	126	4.3	1.9
4Ru-Cl-4Cs-Cl	115	4.5	2.3
4Ru-N-4Cs-Cl	135	4.0	1.9
4Cs-Cl	-	-	-
4Cs-NO	-	-	-

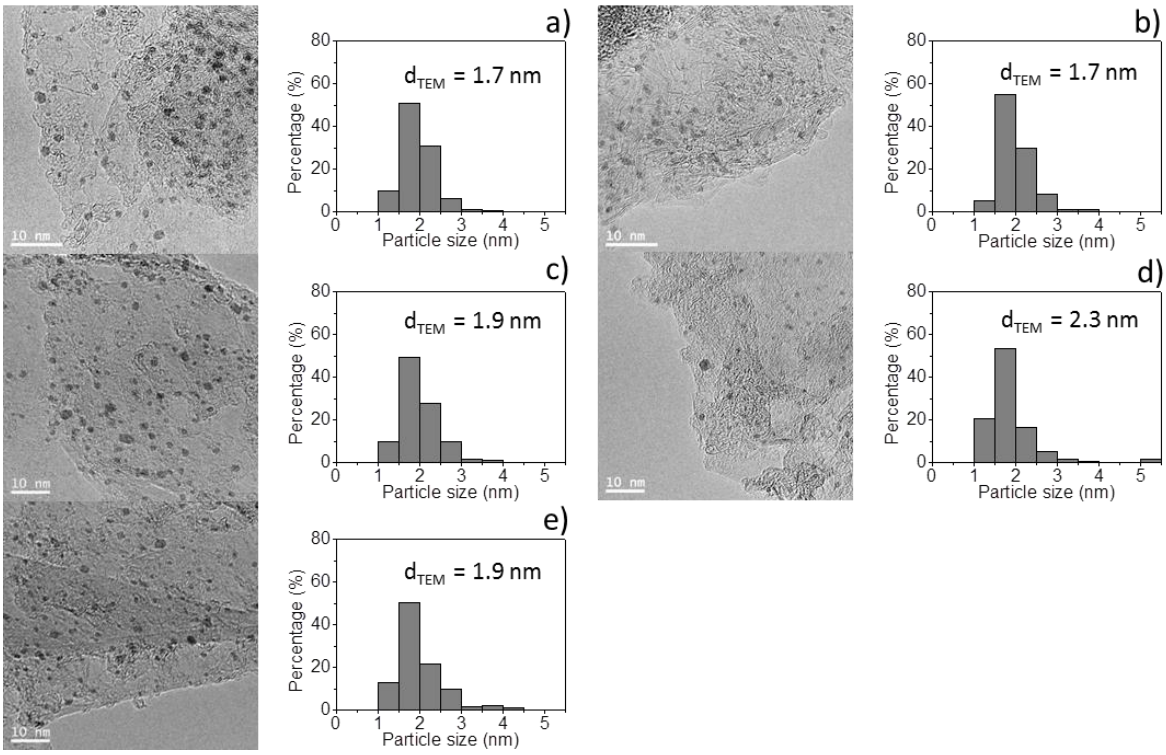

Figure 3. TEM images and particle size distribution of reduced Ru catalysts. (a) 4Ru-N, (b) 4Ru-Cl, (c) 4Ru-N-4Cs-N, (d) 4Ru-Cl-4Cs-Cl and (e) 4Ru-N-4Cs-Cl.

In-situ Ru K-edge XANES spectra during the temperature programmed reduction are compiled in Figure 4. Above 393-473 K, a decreasing intensity of the white line and a shift of the absorption edge toward lower energies are observed obtaining a spectrum similar to that of Ru^0. The sets of XANES were examined by principal component analysis (PCA) to interpret the reduction process [32,33]. By means of PCA is possible to determine the number of Ru chemical species and quantify their concentration during the reduction process. Figure 5 presents the concentration profiles and XANES spectra corresponding to the pure chemical species of Ru observed during the H_2-TPR experiments. Thus, this indicates two Ru chemical species in the samples 4Ru-N and 4Ru-N-4Cs-N, respectively, during the H_2 treatment. In the case of the 4Ru-Cl and 4Ru-Cl-4Cs-Cl samples two and three Ru chemical species were detected respectively. The reduction of the 4Ru-Cl-4Cs-Cl catalyst is a more complex process, occurring in two stages with the detection of an intermediate component as it was demonstrated previously [13]. The formation

of an intermediate Ru oxidized species at low temperatures for the sample 4Ru-Cl-4Cs-Cl suggests a modification of the electronic properties of Ru entities via interaction with the Cs atoms. Also this behavior indicates that an intimated contact of the Ru nanoparticles and the Cs promoter entities takes place during the reduction process.

In order to determine the oxidation state of the different Ru chemical species, some Ru references were analyzed by XANES representing the edge position versus the oxidation state (presented as Figure 6). Below 673 K (reduction temperature for FTS) the total reduction of Ru is achieved for all the catalysts.

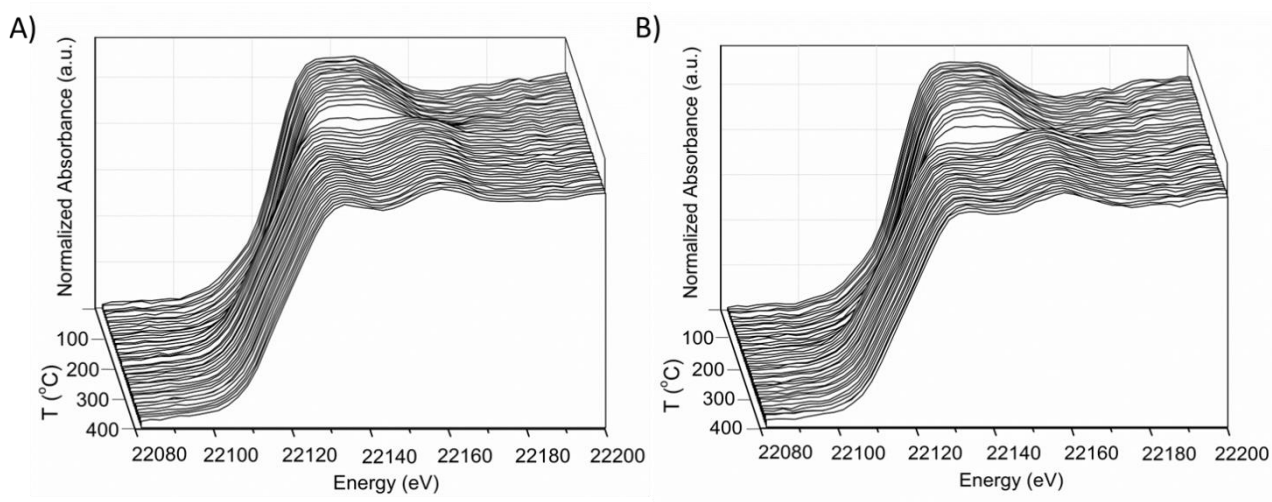

Figure 4. Ru K-edge XANES spectra collected at different temperatures during the reduction process. (A) 4Ru-N, (B) 4Ru-N-4Cs-N. The spectra of 4Ru-Cl and 4Ru-Cl-4Cs-Cl have been provided in a previous study [13].

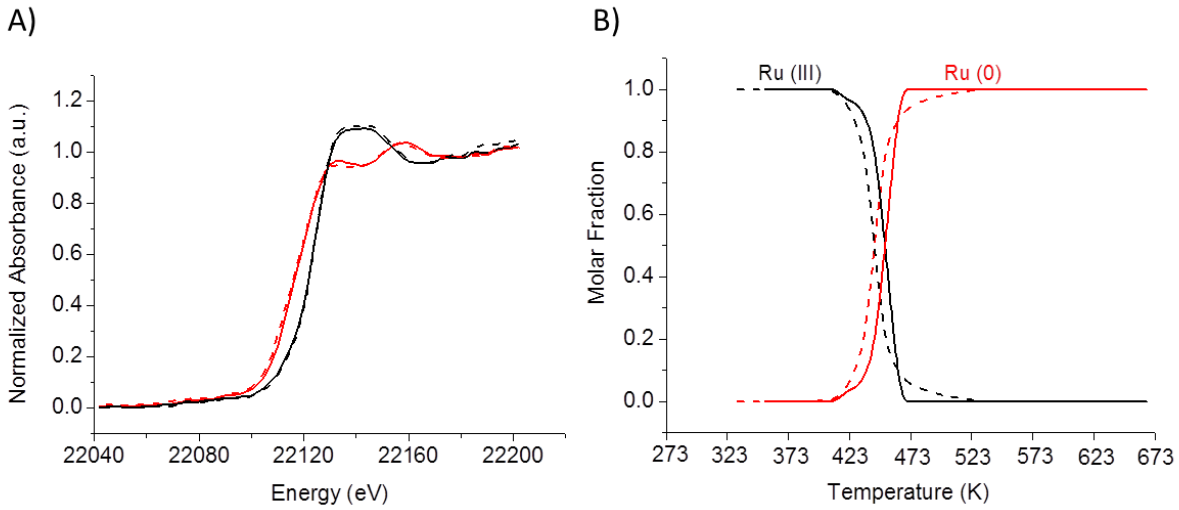

Figure 5. Ru K-edge XANES spectra and concentration profiles obtained by PCA corresponding to pure chemical species along H_2-TPR until 673 K for 4Ru-N (solid line) and 4Ru-N-4Cs-N (dashed line) catalysts.

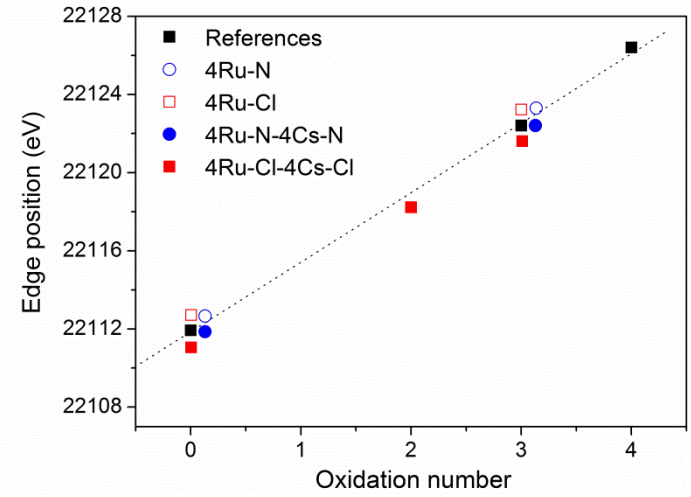

Figure 6. Edge position of pure species from FA for 4Ru-N, 4Ru-Cl, 4Ru-N-4Cs-N and 4Ru-Cl-4Cs-Cl catalysts versus oxidation number of selected references: Ru (foil), $RuCl_3$ and RuO_2.

The Cs L_1 edge XANES spectra recorded during the temperature-programmed reduction for the promoted catalysts 4Ru-Cl-4Cs-Cl and 4Ru-N-4Cs-N are reported in Figure 7. It can be noticed

that the non-reduced samples give rise to a sharp feature at approximately 5712 eV. For the sample 4Ru-Cl-4Cs-Cl, as already reported [13], the white line intensity suffers a severe decrease attributed to an increase of the d state electron density involved in the 2s-3d resonance transition. In addition, a significant 0.68 eV shift of the absorption edge toward lower energies was observed after reduction at 673 K. The study concludes [13], in agreement with other authors [31], that partial reduction of CsCl is produced by H species coming from the dissociative chemisorption of H_2 on Ru. By contrast, for the 4Ru-N-4Cs-N sample a spectra with nearly equal edge shape and with identical absorption edge energy values (a shift < 0.26 eV) was observed during temperature programmed reduction treatment in hydrogen (see Figure 7B). On the other hand, Ru-free Cs blank samples (not shown for the sake of brevity) showed XANES spectra with shapes similar to those corresponding to the 4Ru-N-4Cs-N sample, without any change during temperature programmed reduction treatment in hydrogen. This can be interpreted considering that the $CsNO_3$ decomposition originates a mixture of CsOH and Cs_2O species over the catalyst surface and these species seem to be more hardly reduced than CsCl preventing the cesium partial reduction.

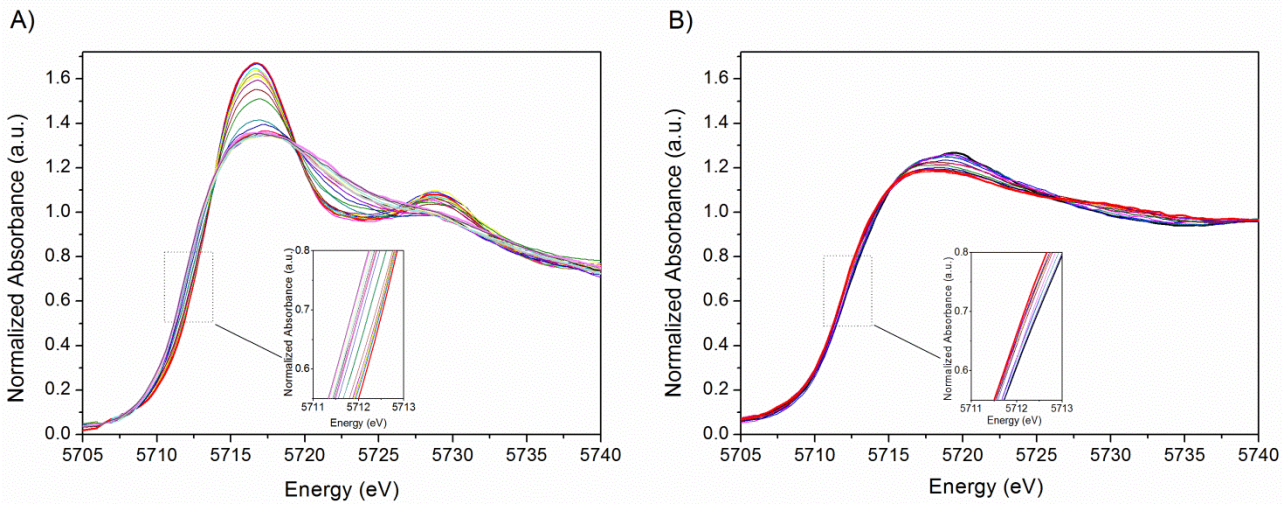

Figure 7. Cs L_1–edge XANES spectra collected during temperature programmed reduction in hydrogen and inset showing an enlargement of their absorption edges at the inflection point for 4Ru-Cl-4Cs-Cl (A) and 4Ru-N-4Cs-N (B) catalysts.

3.2 Fischer-Tropsch Synthesis

Promoted and unpromoted catalysts were tested at 523 K and 3.5 bar for the Fischer-Tropsch reaction to determine the effect of metal and promoter precursors. The evolution of CO conversion as a function of the reaction time is plotted in Figure 8. Most of the catalysts showed a slight decrease in activity during the first 4 hours of reaction before reaching stability, which is maintained during the time studied.

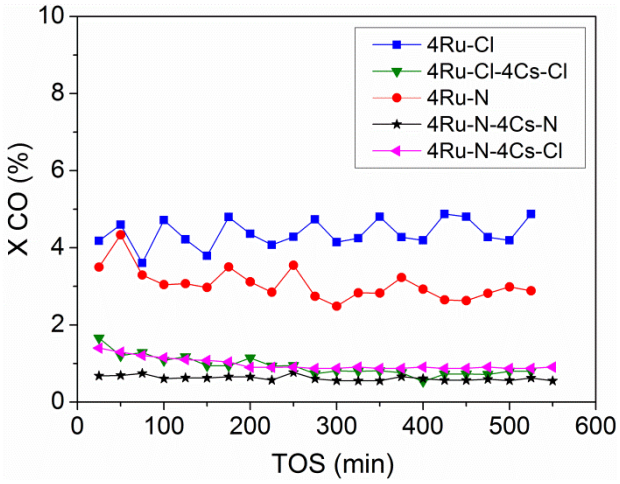

Figure 8. Time-on-stream (TOS) evolution of CO conversion during FTS at 523 K, 3.5 bar, flow rate = 45 cm^3 min^{-1} and $H_2/CO = 2$.

Steady-state catalytic results are compiled in Table 3 for all the catalysts. A comparison of the two unpromoted Ru catalysts reveals that they have basically the same catalytic activity but there are some differences in the product distribution. So, ex-chloride Ru catalyst shows higher selectivity for methane formation and lower olefin to paraffin ratio in the range of C_2–C_3 hydrocarbons. This agrees with earlier literature report [34] where the influence of the chlorine ions presence in Ru/SiO_2 catalysts for the FTS was studied. In our case only traces of chloride (as revealed by XPS analysis) remain on the reduced catalyst, therefore, no loss of activity with respect to the ex-nitrate catalyst was observed. The differences in product selectivity between the two Ru

catalysts can be interpreted taking into account the above discussed microcalorimetry experiments. These latter show that CO adsorption heats for 4Ru-N sample are higher than for 4Ru-Cl for the whole coverage range which could imply that the dissociative adsorption of CO is easier on the former. Typical product composition in the Fischer−Tropsch reaction is described by the Anderson−Schulz−Flory distribution [1, 2]. Following this latter, long-chain-hydrocarbon formation involves the polymerization of CH_x species, formed from CO dissociation and subsequent C hydrogenation [35]. According to this mechanism the surface concentration of CH_x species and hydrogen atoms determine the growth of the hydrocarbon chain and the formation of paraffin or olefins. Therefore, the stronger CO adsorption for the 4Ru-N catalyst measured by microcalorimetry can be related with a higher population of adsorbed dissociative CO and the formation of CH_x species (which helps to increase the rate of C-C coupling [36]) on the catalyst surface, favoring the chain growth and the olefin formation. This reasoning is particularly evident when Cs is added to the Ru catalysts (compare 4Ru-N vs. 4Ru-N-4Cs-N and 4Ru-Cl vs. 4Ru-Cl-4Cs-Cl). The role of Cs promoter is evidenced by the lower activity for CO conversion, the increase of light olefins selectivity, the minor methane production and the increased chain growth probability (α) compared with the non-promoted catalyst for each pair of catalysts, independently of the precursor used. This kind of promotional effect (the so-called electronic effect) has been commonly observed for FTS catalysts involving group VIII metals [8,9,10,11,12]. This result is consistent with the increase in the CO adsorption heats by the presence of cesium compared to the non-promoted Ru catalyst observed by microcalorimetry (Figure 2). It is worth noting that comparing the two Cs promoted, 4Ru-Cl-4Cs-Cl and 4Ru-N-4Cs-N, catalysts only the latter produce an appreciable amount of CO_2. According to the literature [9, 37, 38], the action of alkaline in FTS is not only promoting the formation of C-C bonds, but also enhancing the water gas shift (WGS) reaction. The vast majority of the alkali promoted catalysts studied for FTS contains the alkali oxide. The TPR-XANES of our two promoted catalysts showed that Cs in the reduced 4Ru-

Cl-4Cs-Cl sample is as partially reduced CsCl, whereas in the reduced 4Ru-N-4Cs-N it is present in an oxygen environment as Cs_2O phase. These results indicate that though CsCl and Cs_2O have similar electro donating properties as revealed for their equal impact on the hydrocarbon distribution, only the Cs_2O enhance the activity for the WGS reaction. Therefore, throughout the pretreatment step in hydrogen atmosphere at 673 K of the 4Ru-N-4Cs-N catalyst, ruthenium precursor is decomposed liberating NO_x species. Also, cesium nitrate is decomposed remaining as a mixture of CsOH and Cs_2O species, which would bring the water molecules (produced during FT) closer and then they might interact with the adsorbed CO molecules on the Ru nanoparticles. The promoting effect of alkine oxides accelerating the WGS has been repeatedly reported. J.M. Campbell et al. [39] demonstrated that Cs introduction into Cu(110) enhanced the WGS rate by a factor of 5, due to the enhancement of H_2O byproduct activation over Cs. It was affirmed that a mixture of cesium-oxygen is present under reaction conditions. Richard G. Mallinson and coworkers also observed a high intrinsic activity for WGS when 2-4 wt% of Na was added to Pt particles [40]. Pt-NaO_x interactions provide highly active sites for the WGS reaction at the periphery of the Pt–NaO_x interface and also inhibit Pt particles from sintering. In order to further explore this phenomenon, an additional Cs promoted Ru catalyst was prepared using the ruthenium nitrate precursor but in this case it was promoted with the cesium chloride salt (Table 3, 4Ru-N-4Cs-Cl catalyst). It was observed that the CO_2 selectivity, mainly produced through WGS, significantly decreases, passing from 42 % to 7 % the CO_2 production. Moreover, 4Ru-N-4Cs-Cl catalyst has a FTS performance identical to the 4Ru-Cl-4Cs-Cl and therefore, Cs remains as partially reduced CsCl presumably in both catalysts.

Table 3. Catalytic performance in the Fischer–Tropsch synthesis of Ru and Ru-Cs catalysts at 523 K and 3.5 bar.

3.5 bar	4Ru-N	4Ru-Cl	4Ru-N-4Cs-N	4Ru-N-4Cs-Cl	4Ru-Cl-4Cs-Cl
activity (µmol/(g_{Ru} s))	6.2	8.5	1.0	2.1	2.0
CO conversion (%)	3.6	4.3	0.6	1.1	1.0
CO_2 selectivity (%)	6	2	42	7	7
TOF_{TEM} (s^{-1}) x 10^4	8.1	11.1	1.5	3.5	3.1
product distribution					
CH_4	72	82	46	65	63
C_2-C_6	28	18	54	35	37
α^a	0.57	0.56	0.68	0.62	0.64
O/P^b	0.3	0.1	3.4	2.3	2.8

Reaction conditions: CO/H_2/He (5/10/30, flow rate 45 mL/min), pressure 3.5 bar, temperature 523 K, catalyst (0.5 g), TOS 9 h. [a]The α value was calculated using the Anderson−Schulz−Flory (ASF) distribution in the hydrocarbon range of C_2–C_6. [b]The O/P value was calculated from the ratio of olefin divided by paraffin in the range of C_2–C_3 hydrocarbons.

Additional tests were carried out at medium pressure, 15 bar, to observe the performance of promoted and non-promoted catalysts under industrially relevant conditions. Figure 9 shows the time-on-stream (TOS) evolution of CO conversion during 50 h, where it is revealed that all the catalysts are stable throughout the studied reaction time. The maintained stability during 50 h fully supports the non-occurrence of the undesirable Boudouard reaction [3], which leads to the deposition of carbon blocking the active sites.

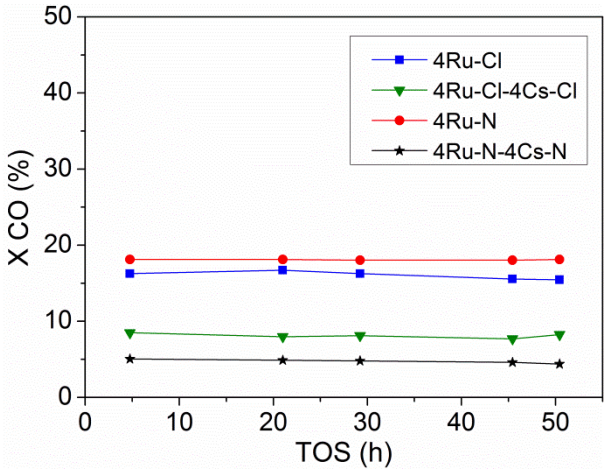

Figure 9. Time-on-stream (TOS) evolution of CO conversion during FTS at 523 K, 15 bar, flow rate = 45 cm^3 min^{-1} and H_2/CO = 2.

Catalytic properties at 15 bar for promoted and unpromoted Ru catalysts are presented in Table 3. It is observed an enhancement of both, the chain-growth probability (α) and the olefin selectivity (higher O/P ratio) by effect of the higher reaction pressure. In addition, the WGS reaction is diminished whereas the FT activity is enhanced, which is particularly evident for the 4Ru-N-4Cs-N catalyst.

Table 4. Catalytic performance in the Fischer–Tropsch synthesis of Ru and Ru-Cs catalysts at 523 K and 15 bar.

15 bar	4Ru-N	4Ru-Cl	4Ru-N-4Cs-N	4Ru-Cl-4Cs-Cl
activity (μmol/(g_{Ru} s))	124	107	26	57
CO conversion (%)	18.1	15.5	4.4	8.2
CO_2 selectivity (%)	1	0	26	5
TOF_{TEM} (s^{-1}) x 10^3	16.1	14.0	3.8	10.1
product distribution				
CH_4	38	49	24	11
C_2-C_6	51	34	51	33
C_{7+}	11	17	25	56
α^a	0.68	0.76	0.86	1.0
O/P[b]	2.10	0.97	3.40	3.15

Reaction conditions: CO/H_2/He (5/10/30, flow rate 45 mL/min, pressure 15 bar, temperature 523 K, catalyst (0.5 g), 50 h. [a]The α value was calculated using the Anderson−Schulz−Flory (ASF) distribution in the hydrocarbon range of C_2−C_6. [b]The O/P value was calculated from the ratio of olefin divided by paraffin in the range of C_2−C_3 hydrocarbons.

4. CONCLUSIONS

Two different ruthenium and cesium precursors supported on a high surface area graphite material were used to prepare catalysts for application in the Fischer-Tropsch process. TPR experiments showed that cesium promoters shifted the ruthenium reduction temperature toward higher values and it was confirmed that Ru is completely reduced after the pretreatment step in hydrogen at 673 K for 2h for all catalysts. From CO chemisorption microcalorimetry measurements it was concluded that independently of the used metal and promoter precursor, cesium has an important contribution in the electronic properties of ruthenium nanoparticles producing a

strengthening in the Ru-CO bond evidenced by higher CO adsorption heats. In particular, in the case of 4Ru-N-4Cs-N catalyst, the highest values of CO adsorption heats (throughout the analysis) were obtained due to the non-presence of residual chlorine species, since these latter withdraw electron density from the ruthenium nanoparticles decreasing the CO adsorption heats. Fischer-Tropsch reaction results revealed that all catalysts were stable throughout the experiment and therefore, the occurrence of the Boudouard reaction is discarded. The role of Cs was evidenced by an increase of the olefins-paraffins ratio, by a decrease in the methane production and consequently by higher formation of long-chain-hydrocarbons, either olefins or paraffins. Interestingly, the 4Ru-N-4Cs-N catalyst provided a high value of CO_2 production which can be related with its catalytic activity for WGS reaction. XANES analysis at Cs L_1 edge was recorded during the temperature-programmed reduction, observing a partial reduction of the CsCl species for the 4Ru-Cl-4Cs-Cl catalyst. By contrast, for the 4Ru-N-4Cs-N sample similar Cs spectrum with equal absorption edge energy values were observed along all the H_2 TPR which is attributed to the formation of hardly reducible CsOH and Cs_2O species over the catalyst surfaces as consequence of the $CsNO_3$ precursor decomposition. These species are able to adsorb water molecules (co-product of the FT reaction), and then these water intermediates can interact with the CO molecules adsorbed on the Ru nanoparticles improving the WGS reaction and giving place to undesired production of CO_2.

ACKNOWLEDGMENT

We acknowledge financial support from the Spanish Government (projects CTQ2014-52956-C3-2-R and CTQ2014-52956-C3-3-R) and thanks CSIC for PIM-2014-201480I012 project. The ESRF and ALBA synchrotron are thanked for granting beamtime at ID24 and BL22-CLAESS, respectively.

REFERENCES

[1] H. Schulz, *Appl. Catal. A: Gen*. 186 (1999) 3–12.

[2] G.P. van der Laan, A.A.C.M. Beenackers, Catal. Rev. Sci. Eng. 41 (1999) 255–318.

[3] M. E. Dry, Catal. Today 71 (2002) 227–241.

[4] M. Gharibi, F. T. Zangeneh, F. Yaripour, S. Sahebdelfar, Appl. Catal. A 443-444 (2012) 8-26.

[5] Q. Zhang, J. Kang, V. Wang, ChemCatChem. 2 (2010) 1030–1058.

[6] D. A. Simonetti, J. Rass-Hansen, E. L. Kunkes, R. R. Soares, J. A. Dumesic, Green Chem. 9 (2007) 1073–1083.

[7] L. Gonzalo-Chacón, M. Almohalla, E. Gallegos-Suarez, A. Guerrero-Ruiz, I. Rodríguez-Ramos, Appl. Catal. A 480 (2014) 86-92.

[8] T. E. Hoost, J. G. Goodwin Jr, J. Catal. 137, (1992) 22–35.

[9] N. Lohitharn, J. G. Goodwin Jr, J. Catal. 260 (2008) 7–16.

[10] M. Guraya, S. Sprenger, W. Rarog-Pilecka, D. Szmigiel, Z. Kowalczyk, M. Muhler, Appl. Surf. Sci. 238 (2004) 77–81.

[11] K. Aika, K. Shimazaki, Y. Hattori, A. Ohya, S. Ohshima, K. Shirota, A. Ozaki, J. Catal. 92 (1985) 296–304.

[12] Z. Kowalczyk, M. Krukowski, W. Raróg-Pilecka, D. Szmigiel, J. Zielinski, Appl. Catal. A 248 (2003) 67-73.

[13] J. L. Eslava, A. Iglesias-Juez, G. Agostini, M. Fernández-García, A. Guerrero-Ruiz, I. Rodríguez-Ramos, ACS Catal. 6 (2016) 1437–1445.

[14] S. L. Soled, E. Iglesia, R. A. Fiato, J. E. Baumgartner, H. Vroman, S. Miseo, Top. Catal. 26 (2003) 101–109.

[15] S. Storsæter, B. Tøtdal, J. C. Walmsley, B. S. Tanem, A. Holmen, J. Catal. 236 (2005) 139–152.

[16] H.F. Xiong, H.N. Pham, A.K. Datye, J. Catal. 302 (2013) 93.

[17] K. Xiong, J. L. Li, K. Y. Liew, X. D. Zhan, Appl. Catal., A: Gen. 389 (2010) 173–178.

[18] E. Iglesia, S.L. Soled, R.A. Fiato, J. Catal. 137 (1992) 212-224.

[19] Guczi (Ed.), New trends in CO activation, Studies on Surface Science Catalysis, vol. 64, Elsevier, Amsterdam, 1991, p. 494.

[20] Progress in C1 Chemistry, Kodansha, Tokyo, 1989, p. 394.

[21] M.K. Niemelä, A.O.I. Krause, T. Vaara, J. J. Kiviaho, M. Reinikainen, Appl. Catal. A 147 (1996) 325-345.

[22] E. Iglesia, S. C. Reyes, R. J. Madon, Adv. Catal. 39 (1993) 221.

[23] E. Iglesia, S. L. Soled, R. A. Fiato, G. H. Via, J. Catal. 143 (1993) 345.

[24] R. C. Reuel, C. H. Bartholomew, J. Catal. 85 (1984) 78.

[25] J. Kiviaho, M. K. Niemelä, M. Reinikainen, T. Vaara, T. A. Pakkanen, J. Mol. Catal. A 121 (1997) 1.

[26] M. K. Niemelä, L. Backman, A. O. I. Krause, T. Vaara, Appl. Catal. A 156 (1997) 319.

[27] P. Gallezot, C. Leclercq, In Physical Techniques for Solid Materials. Fundamental and Applied Catalysis, B. Imelik, J. C. Vedrine, Eds., Plenum Press, New York, NY. 1994, p. 509.

[28] J.R. Anderson, Structure of Metallic Catalysts, Academic Press (London), New York, 1975, pp. 289–39

[29] M. Cerro-Alarcón, A. Maroto-Valiente, I. Rodríguez-Ramos, A. Guerrero-Ruiz, Carbon 43 (2005) 2711–2722.

[30] E. Gallegos-Suarez, L. Gonzalo-Chacón, I. Rodríguez-Ramos, A. Guerrero-Ruiz, Thermochim. Acta 567 (2013) 112–117.

[31] I. Rossetti, L. Sordelli, P. Ghigna, S. Pin, M. Scavini, L. Forni, Inorg. Chem. 50 (2011) 3757-3765.

[32] M. Fernandez-García, C. Marquez, G. L. Haller, J. Phys. Chem. 99 (1995) 12565−12569.

[33] C. Marquez-Alvarez, I. Rodríguez-Ramos, A. Guerrero-Ruiz, G. L. Haller, M. Fernández-García, J. Am. Chem. Soc. 119 (1997) 2905−2914.

[34] E. lyagaba, E. Hoost, J. Nwalor and J.G. Goodwin Jr., J. Catal., 123 (1990) 1

[35] R. A. van Santen, I. M. Ciobica, E. van Steen, M. M. Ghouri, Adv. Catal. 54 (2011) 127–187.

[36] J. Chen, Z.-P. Liu, J. Am. Chem. Soc. 130 (2008) 7929-7937.

[37] H.M. Torres-Galvis, KP. De Jong, ACS Catal. 3 (2013) 2130-2149.

[38] Q.H.Zhang, J.C. Kang, Y. Wang, ChemCatChem 2 (12) 10-1058.

[39] J.M. Campbell, J. Nakamura, C.T. Campbell, J. Catal. 136 (1992) 24-42.

[40] X. Zhu, M. Shen, L. L. Lobban, R. G. Mallinson, J. Catal. 278 (2011) 123-132.